Bimetallic gold-silver nanoparticles mediate bacterial killing by disrupting the actin cytoskeleton MreB

Prajna Jena,[*a] Maireyee Bhattacharya,[b] Gourab Bhattacharjee,[c] Biswarup Satpati,[c] Prasun Mukherjee,[a] Dulal Senapati,[*b] Ramanujam Srinivasan[*d]

[a]Centre for research in nanoscience and nanotechnology, University of Calcutta, JD-2, sector -3, Salt Lake City, Kolkata, India

[b]Chemical Sciences Division, Saha Institute of Nuclear Physics, HBNI, 1/AF, Bidhannagar, Kolkata-700064, India

[c]Surface Physics and Material Science Division, Saha Institute of Nuclear Physics, HBNI, 1/AF, Bidhannagar, Kolkata-700064, India

[d]School of Biological Sciences, National Institute of Science Education and Research (NISER), HBNI, Bhubaneswar, Odisha 752050, India

Supplementary Figure Legends and Supplementary Table

Supplementary Figure 1

Fig SI-1. UV-vis-NIR absorption spectra of nanoparticles. A. Au-Ag aggregate NP, Ag NP and Au NP prepared at 70 °C showed an absorption peak at 540 nm, 440 nm and 520 nm respectively. **B**. Au-Ag non-aggregate NP, Ag NP and Au NP synthesized via boiling method (at 100 ^{0}C) displayed absorption peak at 485 nm, 427 nm and 518 nm respectively. Variation in color appearance was observed for Au-Ag NPs synthesized at different temperatures (70 °C vs. 100 °C) as shown in the inset.

Supplementary Figure 2

Fig SI-2. Surface enhanced Raman spectroscopy of nanoparticles. Recorded SERS signals from Rh6G on **A**. Aggregated Au-Ag NP and the corresponding Ag NP and Au NP, **B**. Non-aggregated Au-Ag NP along with Ag NP and Au NP. 671 nm CW laser light was used as the excitation source.

Supplementary Figure 3

Fig SI-3. Adherence of NP on the bacterial surface. Adherence of aggregated Au-Ag NP [**A(i)** and **(ii)**] for 2 and 4 hours respectively in *E. coli* were checked by dehydrating the cells under series of ethanol wash and capturing images in TEM. Similarly, attachment of non-aggregated Au-Ag NP referred to as N-Au-Ag NP [**A(iii)** and **(iv)**] for 2 and 4 hours respectively in *E. coli* were also checked by the same method. Scale bar: 0.5 µm. Number of aggregated and non-aggregated Au-Ag NPs per bacterial cells after 2 and 4 hours as observed from TEM micrographs were counted and plotted (**B**). Mean and SD are shown.

Supplementary Figure 4

Fig SI-4. Antibacterial activities of monometallic and bimetallic NPs. Dose dependent antibacterial activities of non-aggregated Au-Ag NP (referred to as N-Au-Ag) versus aggregated Au-Ag NP against *E.coli* (**A**) and *S. typhimurium* (**D**). Effect of different concentrations of Au NP, Ag NP and mixture of Au NP and Ag NP corresponding to bimetallic Au-Ag NP doses were checked against *E.coli* (**B**) and *S. typhimurium* (**E).** The antibacterial effect of different concentrations of $AgNO_3$ (5 µM, 10 µM and 20 µM) were determined in *E.coli* (**C**) and *S. typhimurium* (**F**). Results are shown with mean SD.

Supplementary Figure 5

Fig SI-5. Time dependant study of cell death. Live-dead staining of *E. coli* MreB-mVenus-^{SW} exposed to 10 , 20 µM Au-Ag NP, A22 and CCCP for 1, 2 and 3 hours followed by staining of the cells with 30 µg/mL PI for 10 min (**A, B and C**). Percentage of dead cells after 1, 2 ,3 and 4 hours of NP, A22 and CCCP treatment are shown(**D**). Mean and SD are plotted. n=100.

Supplementary Figure 6

Fig SI-6. Dissipation of PMF-dependent proteins by Au-Ag NP. A. Cellular delocalization of GFP-FtsA in *E. coli* (GPF-FtsA) strain in presence of proton ionophore CCCP (100µM; 10 min); 100µM of Au-Ag NP for 10 min, and 20 µM of Au-Ag NP for 60 min respectively. **B**. Effect of CCCP (100µM; 10 min) and Au-Ag NP (100 µM; 10 min, 20µM; 60 min) on delocalization of MinD protein of GFP-JunLZ-MTS_{MinD} *E.coli* strain. The fluorescence

intensities of treated and untreated cells of GFP-FtsA and GFP-JunLZ-MTS_{MinD} *E. coli* are measured by drawing a line on cells as indicated. Scale bars: 6 µm and 2 µm for **A** and **B** respectively.

Supplementary Figure 7

Fig SI-7. Effect of NP against *E. coli* mutants with defective membrane. Sensitivity of *E. coli* dcrB mutant showing defective membranes was determined relative to WT *E. coli* with exposure of 5 µM, 10 µM and 20 µM of Au-Ag NP for 4 hours. Serially diluted cells were plated in LB-Agar overnight at 37 ° C, counted and the percentage of survival was determined. Mean and Standard deviation are plotted.

Supplementary Figure 8

Fig SI-8. Effect of Au-Ag NP on FtsZ. **A**. FtsZ rings (shown in GFP panel) with the treatment of 10 µM of NP in *E. coli* cells expressing FtsZ-GFP. Scale bar corresponds to 2 µm. **B**. Percentage of cells with FtsZ rings in untreated cells and cells treated with 10 µM Au-Ag NP.

Supplementary Figure 9

Fig SI-9. Fluorescence intensity profiles of MreB delocalized cells. Quantification of fluorescence of $MreB^{SW}$-mVenus *E. coli* and (**A**) and msfGFP-MreB in *B. subtilis* (**B**) with NP, A22 and CCCP as mentioned. The values plotted in the graphs are the fluorescence intensities of treated and untreated cells measured by drawing cell boundaries.

Supplementary Figure 10

Fig SI-10. Susceptibility of MreB mutant to NP. *E. coli* cell with a point mutation at position A53T was treated with 10 and 20 µM Au-Ag NP for 4 hours to show increased susceptibility of MreB mutant $A53T^{SW}$-mVenus to NP Au-Ag NP. Scale bar: 3 µm.

Supplementary Figure 11

Fig SI-11. Delocalization of MreB with the treatment of 10 µM of NP followed by loss of MreB with 20 µM treatment in *E. coli* cells with $MreB^{SW}$-mVenus at **A**. 30° C and **B**. 42°. Cells were observed in DIC. MreB puncta were represented by the deconvolution method. Scale bar corresponds to 3 µm.

Supplementary Figure 12

Fig SI-12. MreB mutation causes aberrant membrane fluid regions. $MreB^{SW}$-mVenus *E. coli* and *E. coli* mutant $MreBA53T^{SW}$-mVenus were checked for the formation of RIF in absence of Au-Ag NP by the same method as described earlier in **Fig. 8**. MreB is shown in green, nile red in red and the cells were observed in DIC. Scale bar corresponds to 3 µm.

Supplementary Figure 13

Fig SI-13. Time dependant study of the formation of aberrant fluid regions. Formation of regions of increased fluidity (RIF) in *E.coli* $MreB^{SW}$-mVenus exposed to 10 , 20 µM Au-Ag NP, A22 and CCCP for 1, 2 and 3 hours was determined by staining the cells with nile red (2 µg/mL, 5 min) (**A, B and C**). Percentage of nile red positive cells after 1, 2 ,3 and 4 hours of NP, A22 and CCCP treatment are shown(**D**). Mean and SD are plotted. n=100.

Supplementary Table 1

Table S1 - Strain Information. Details of strains used in this study are listed.

Supplementary Figure 1

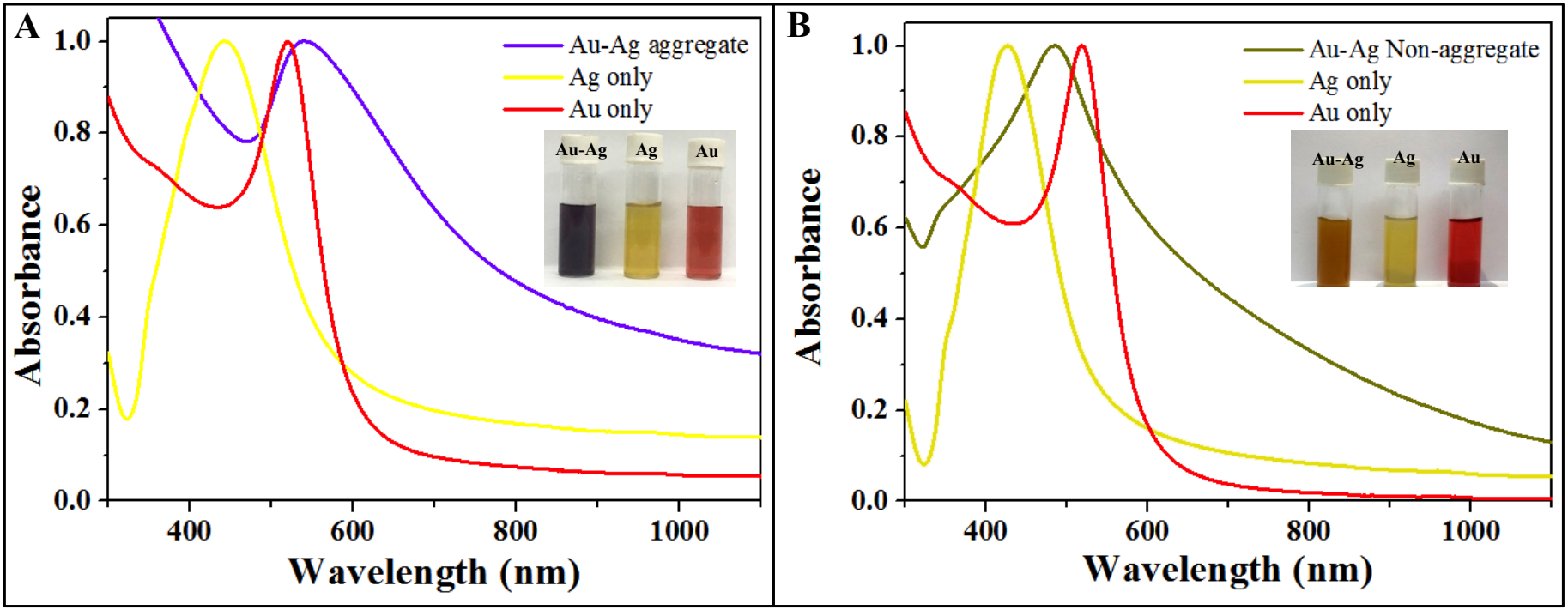

Fig. SI-1.

Supplementary Figure 2

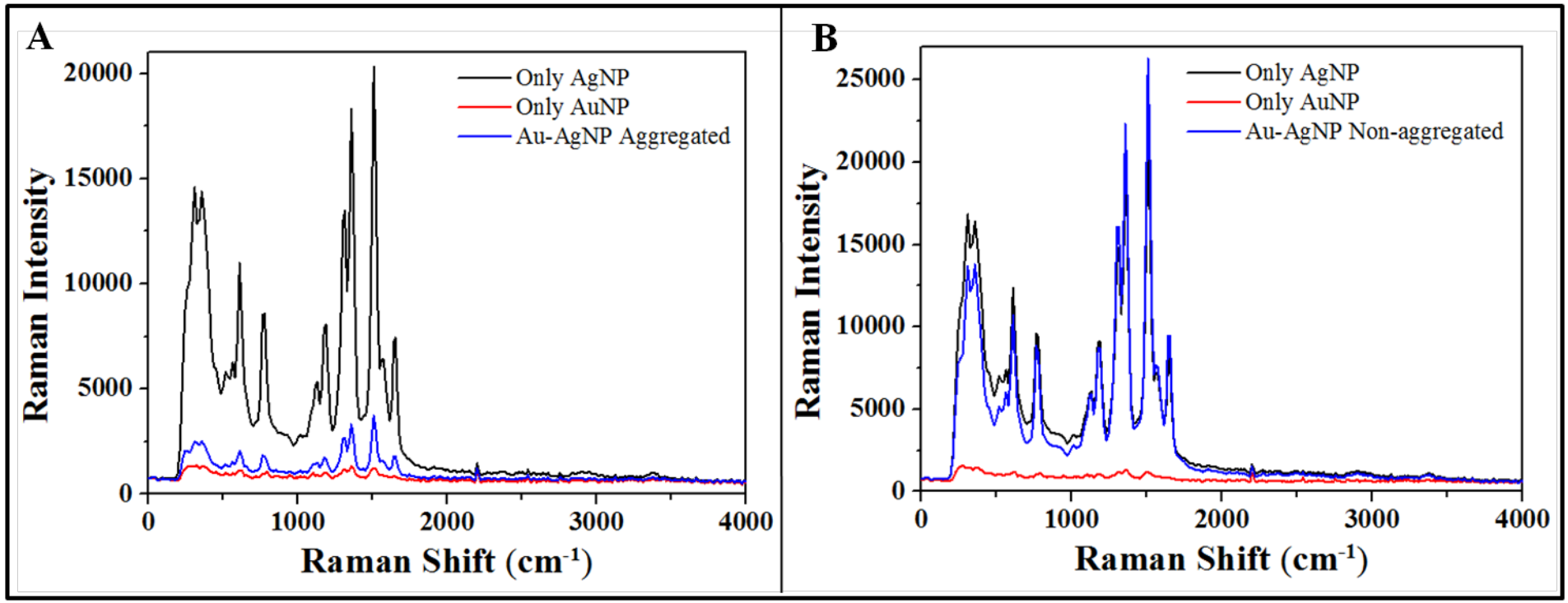

Fig. SI-2.

Supplementary Figure 3

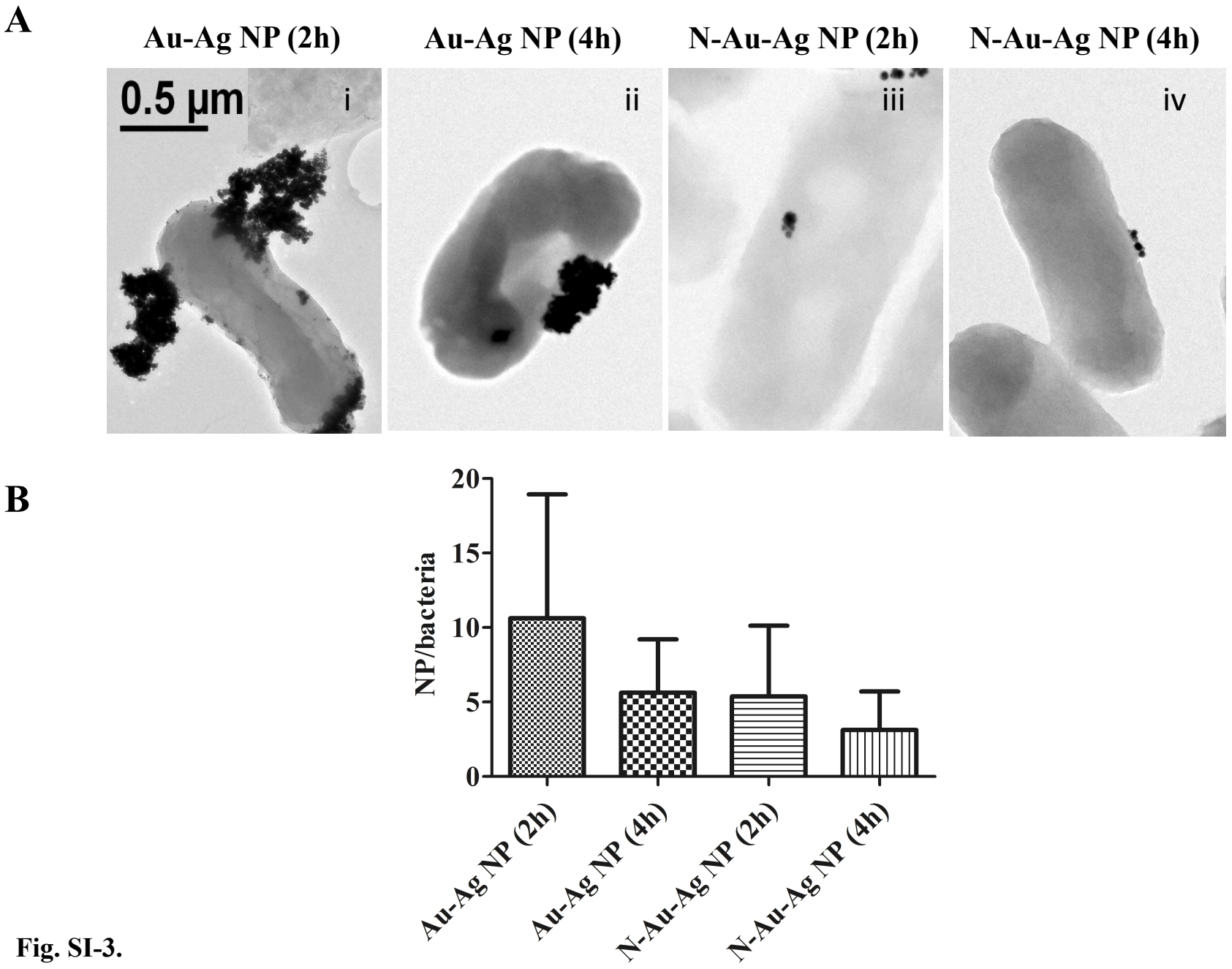

Fig. SI-3.

Supplementary Figure 4

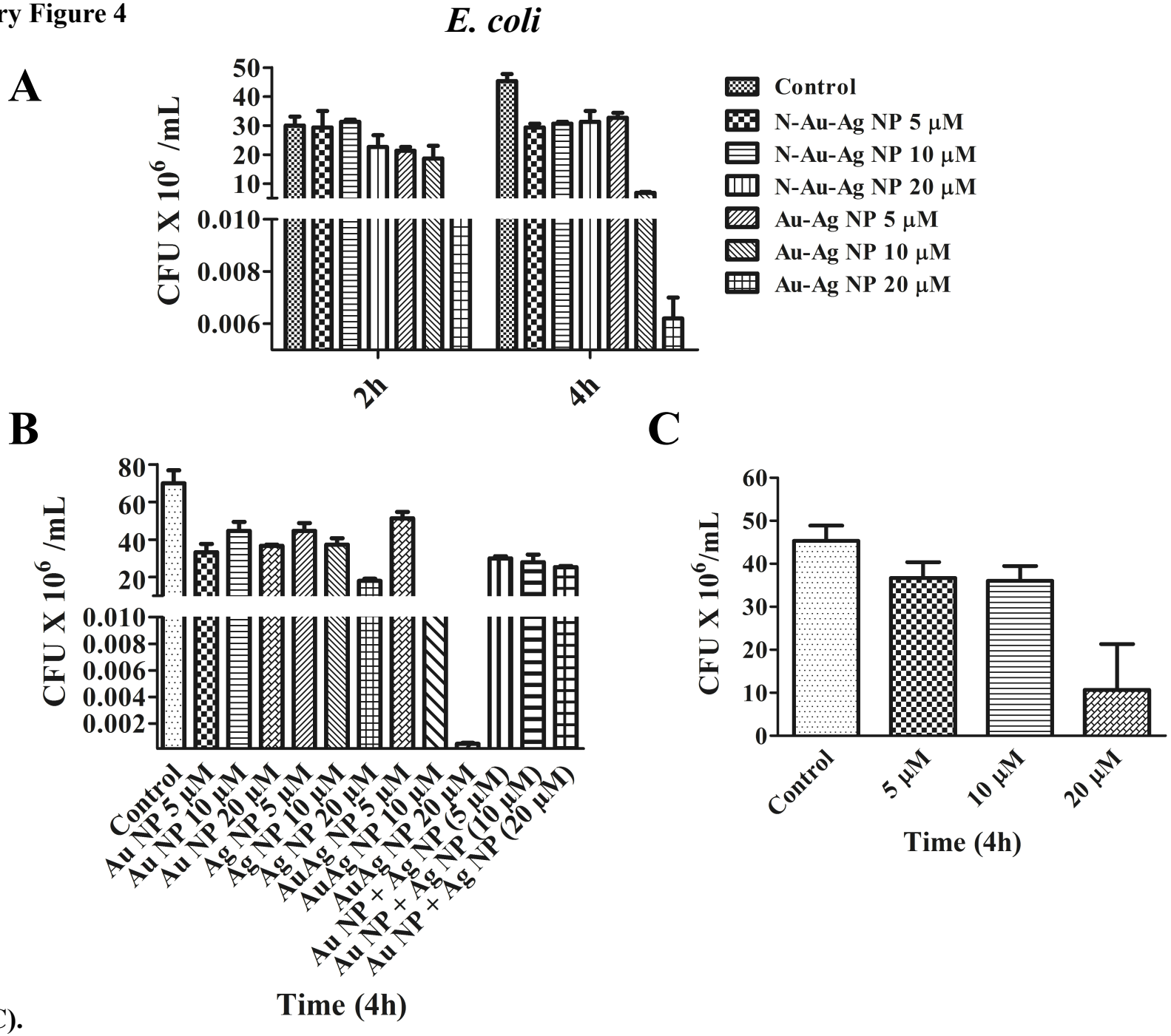

Fig. SI-4 (A-C).

Supplementary Figure 4

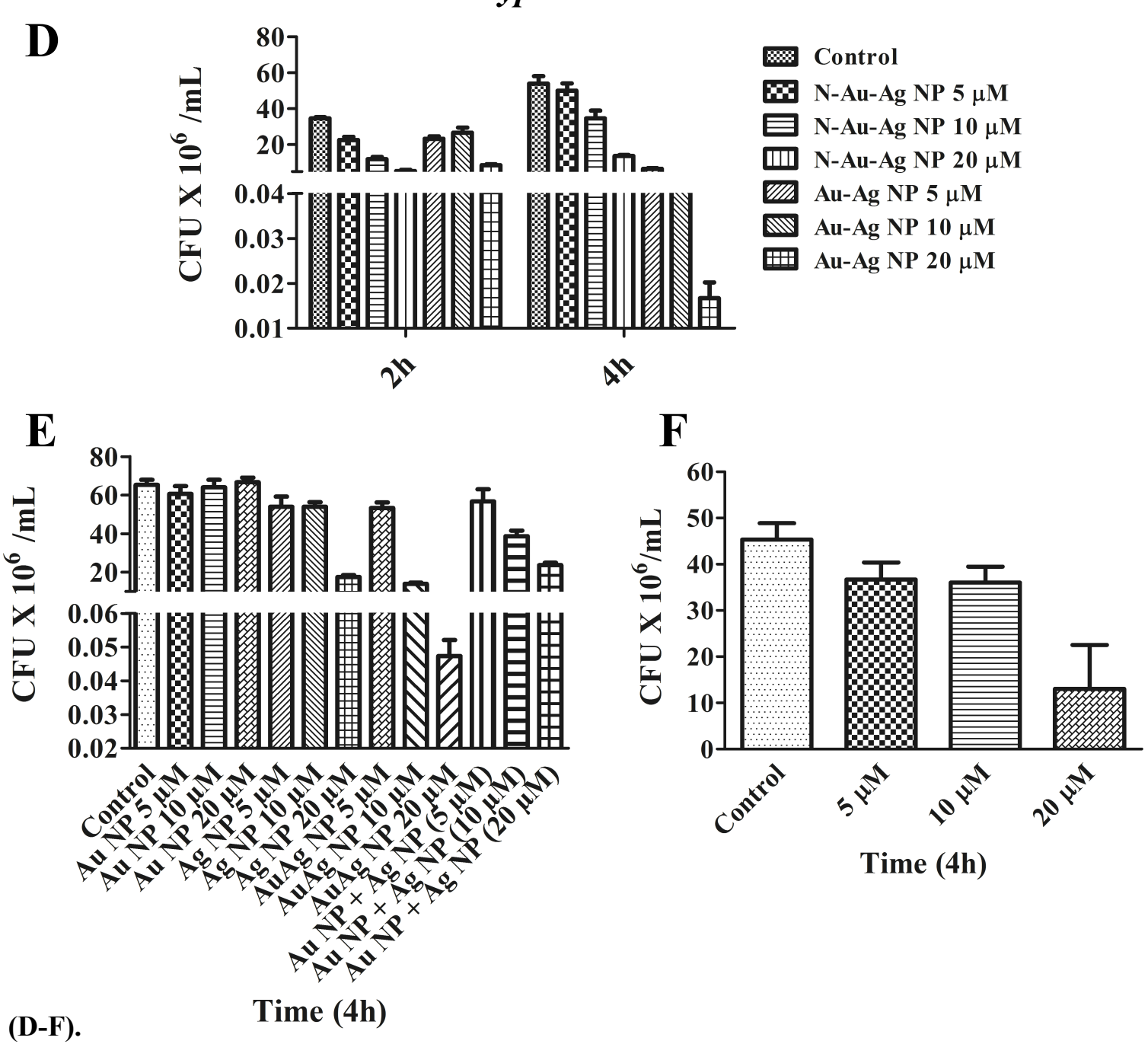

Fig. SI-4 (D-F).

Supplementary Figure 5

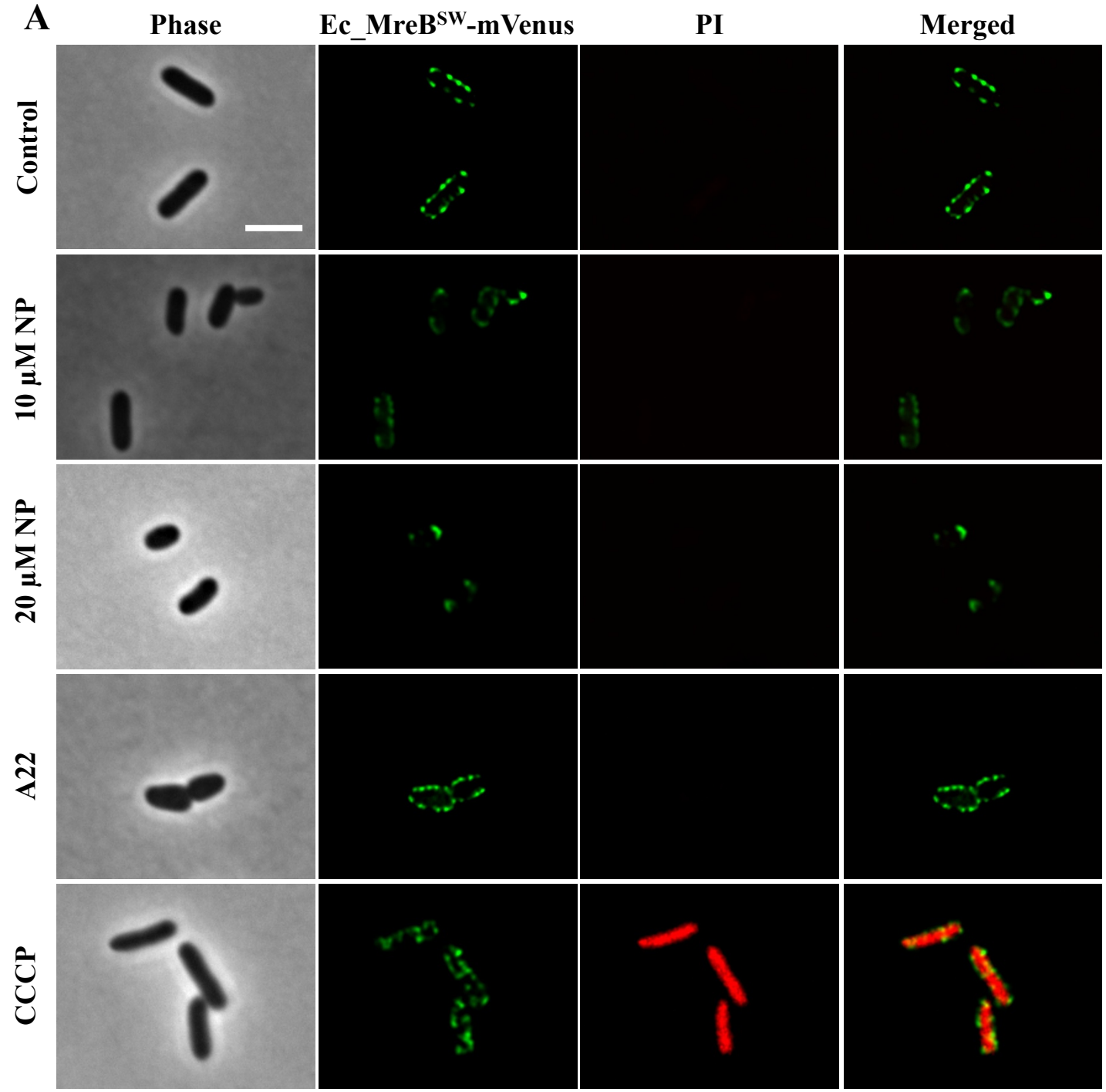

Fig. SI-5A.

Supplementary Figure 5

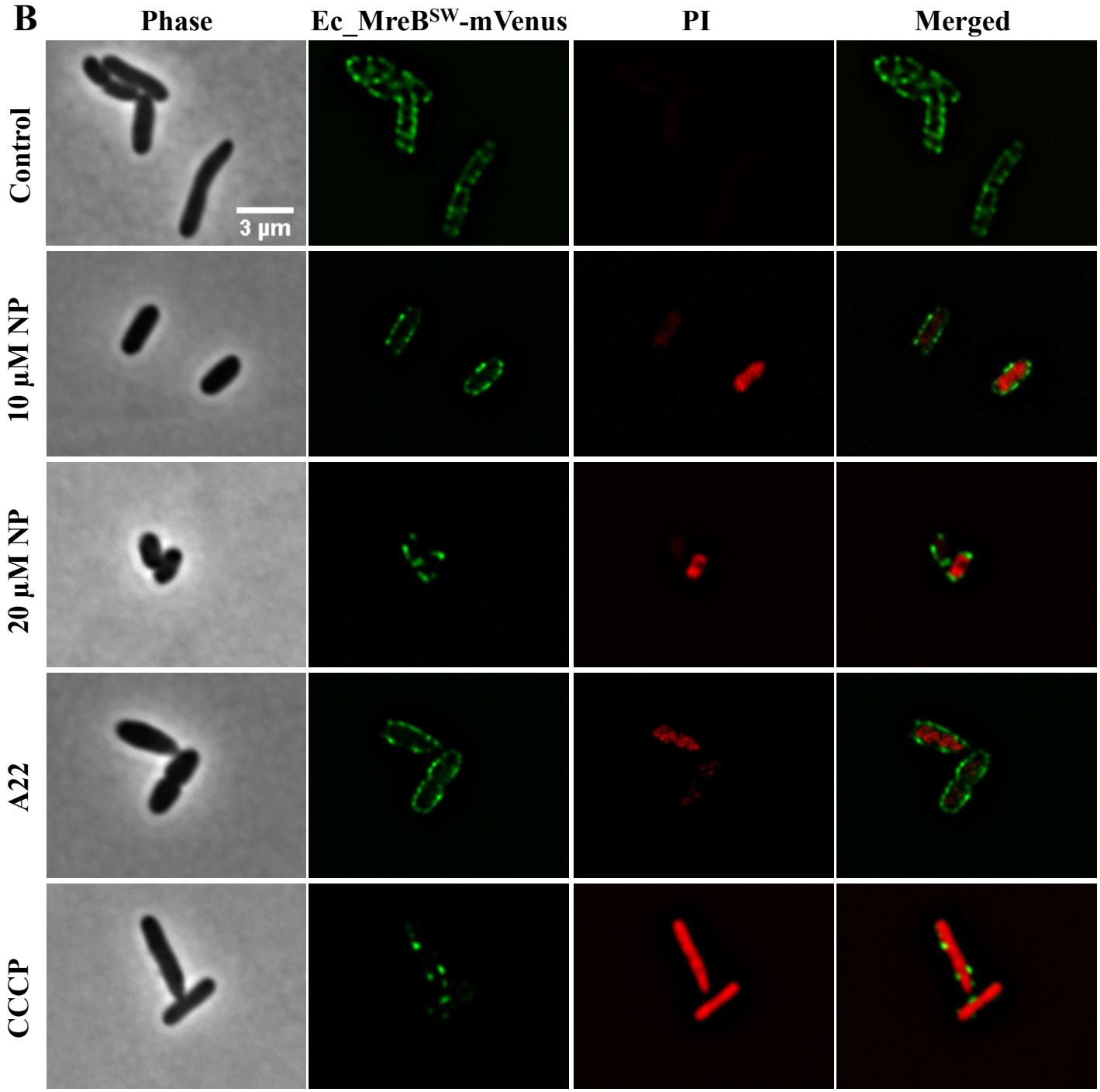

Fig. SI-5B.

Supplementary Figure 5

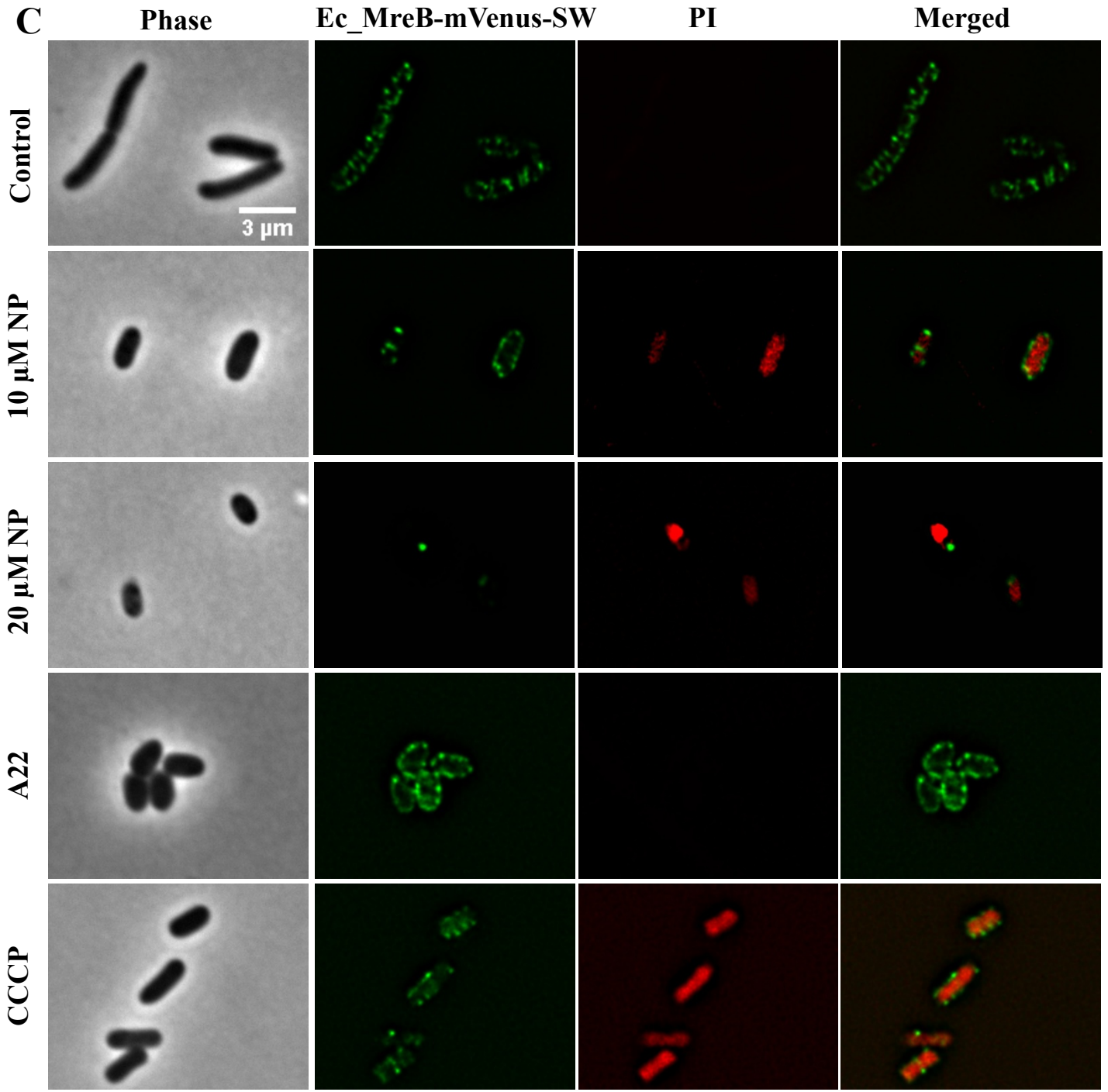

Fig. SI-5C.

Supplementary Figure 5

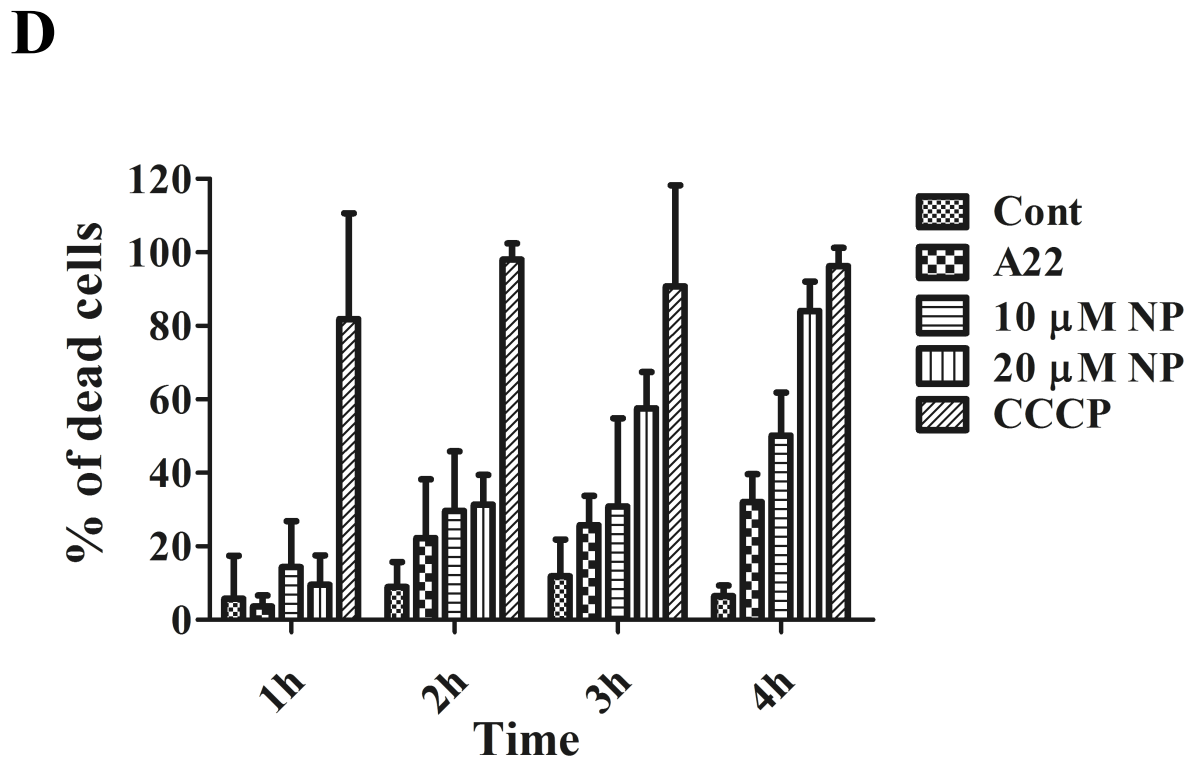

Fig. SI-5D.

Supplementary Figure 6

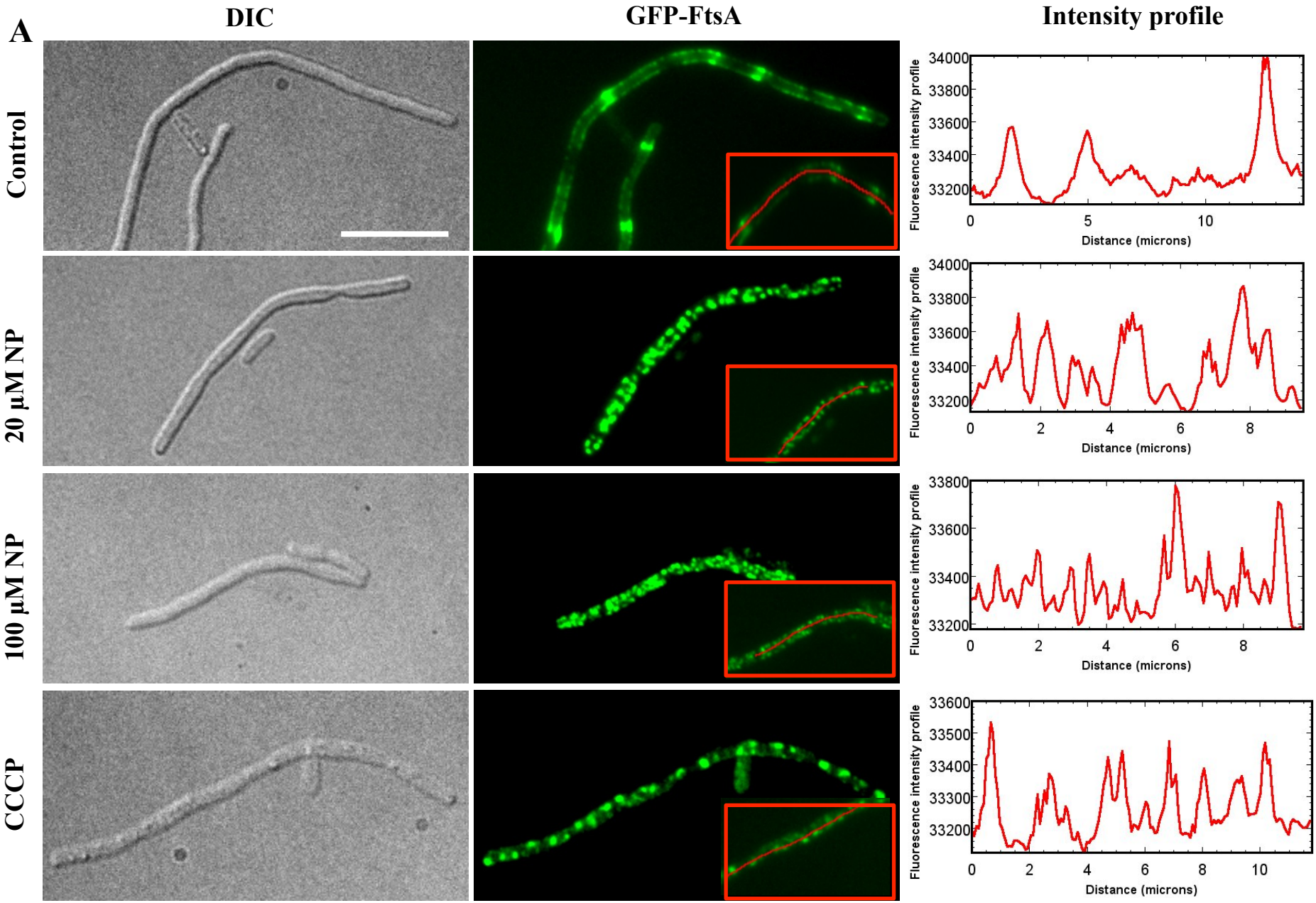

Fig. SI-6A.

Supplementary Figure 6

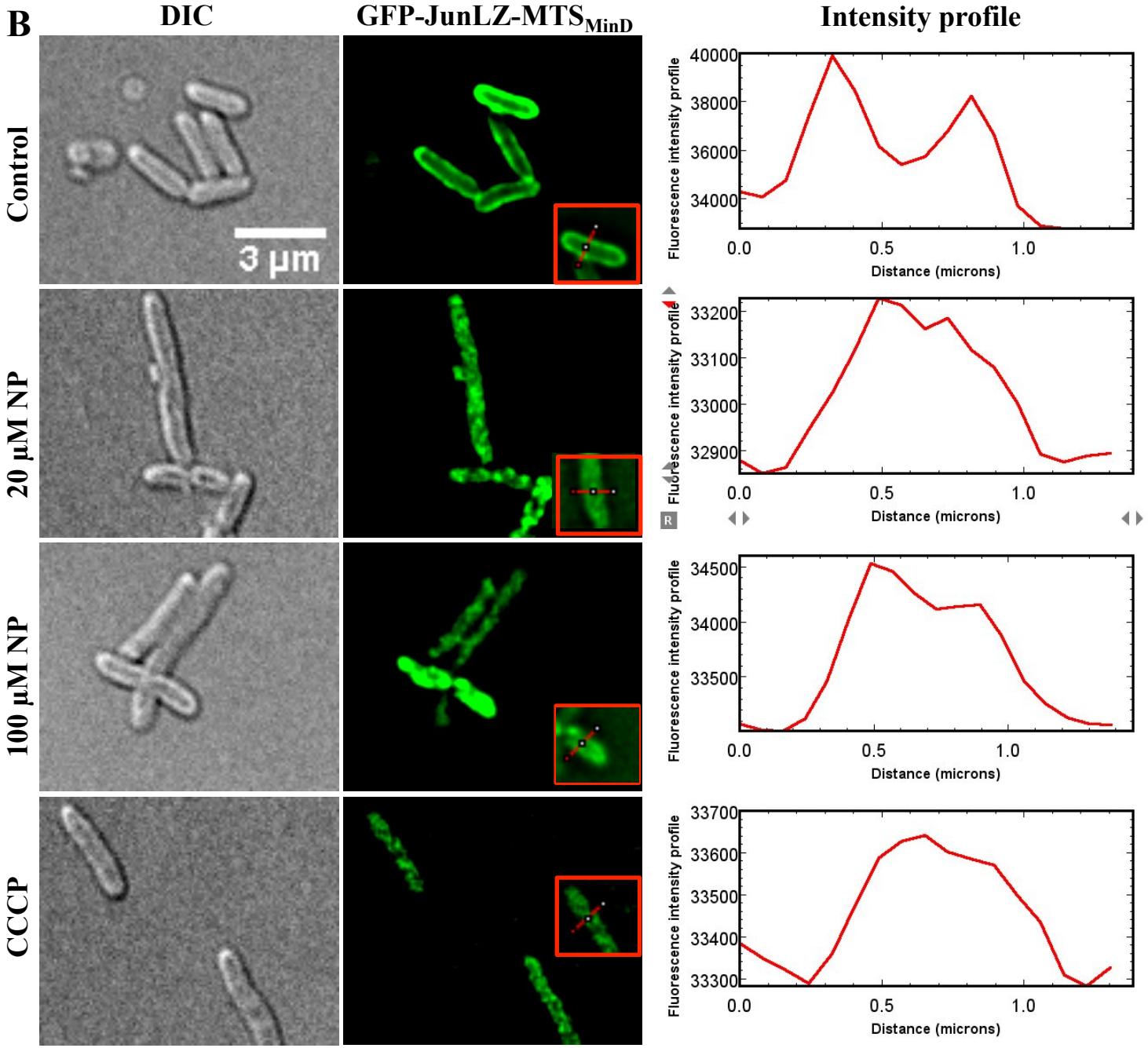

Fig. SI-6B.

Supplementary Figure 7

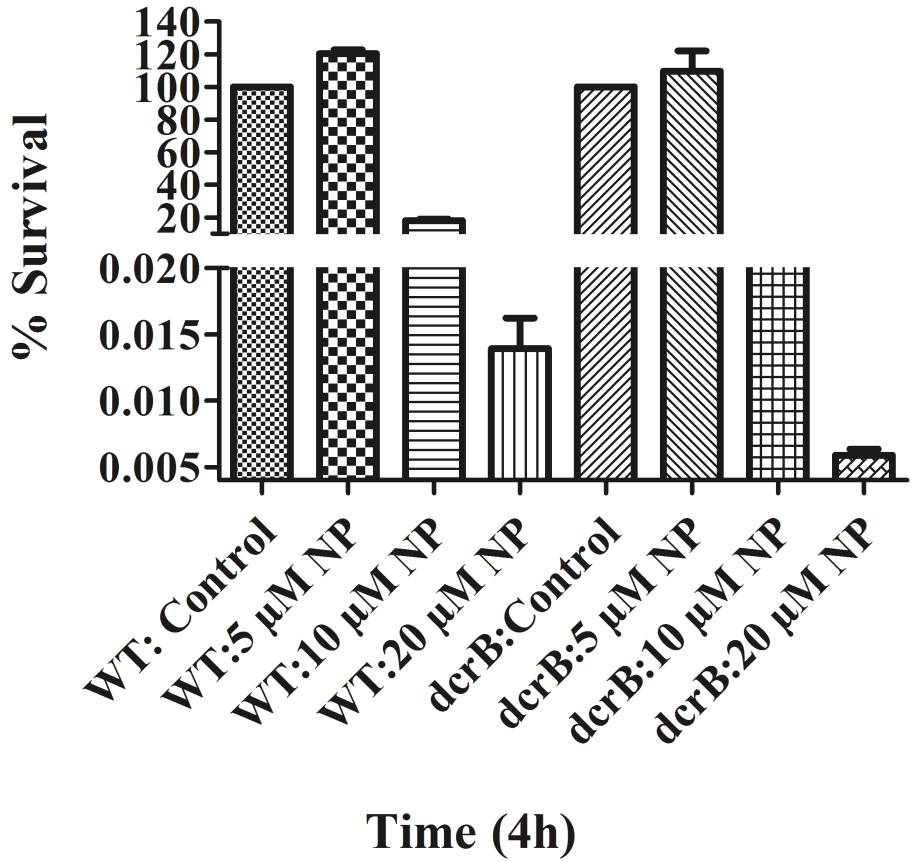

Fig. SI-7.

Supplementary Figure 8

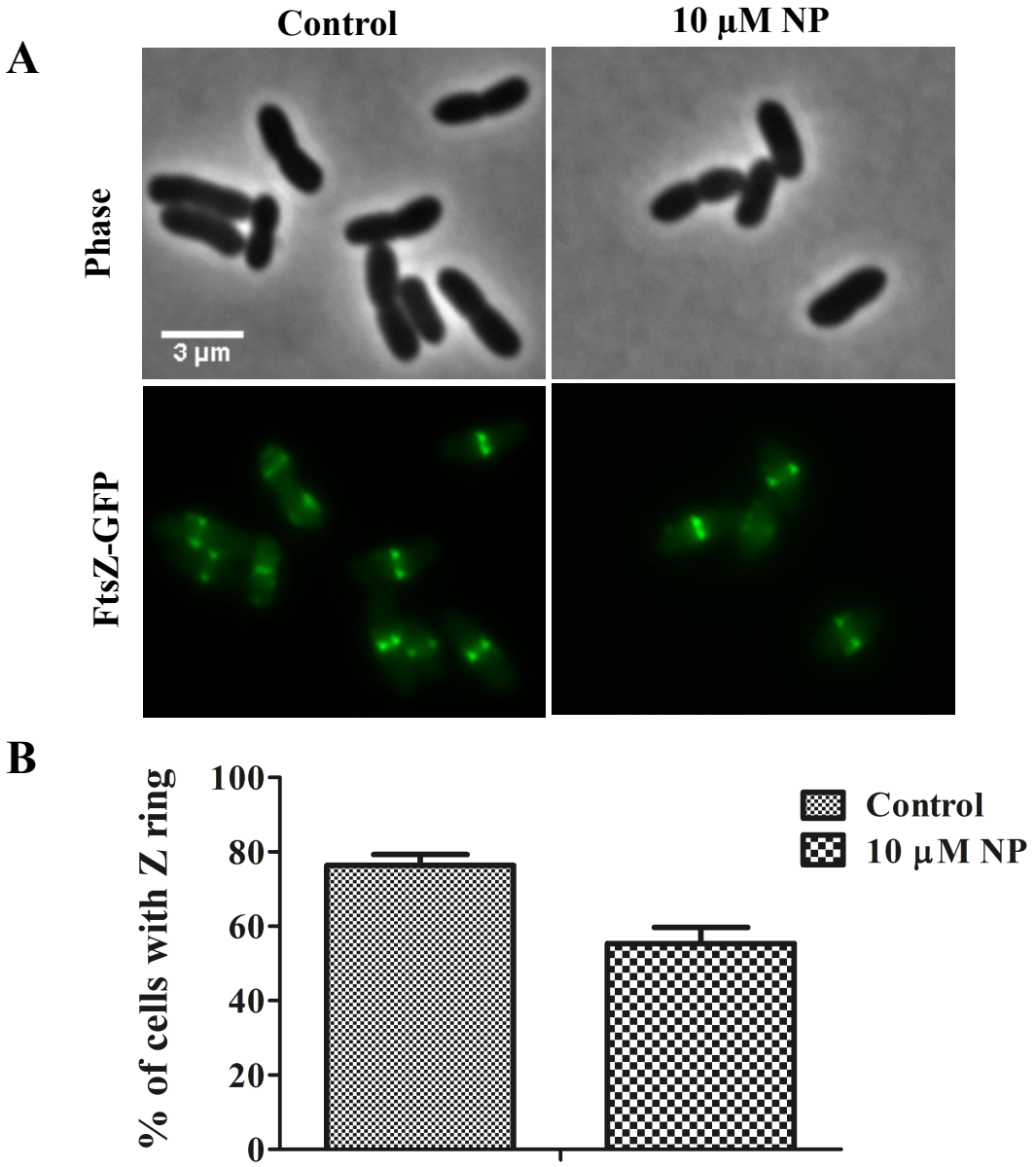

Fig. SI-8.

Supplementary Figure 9

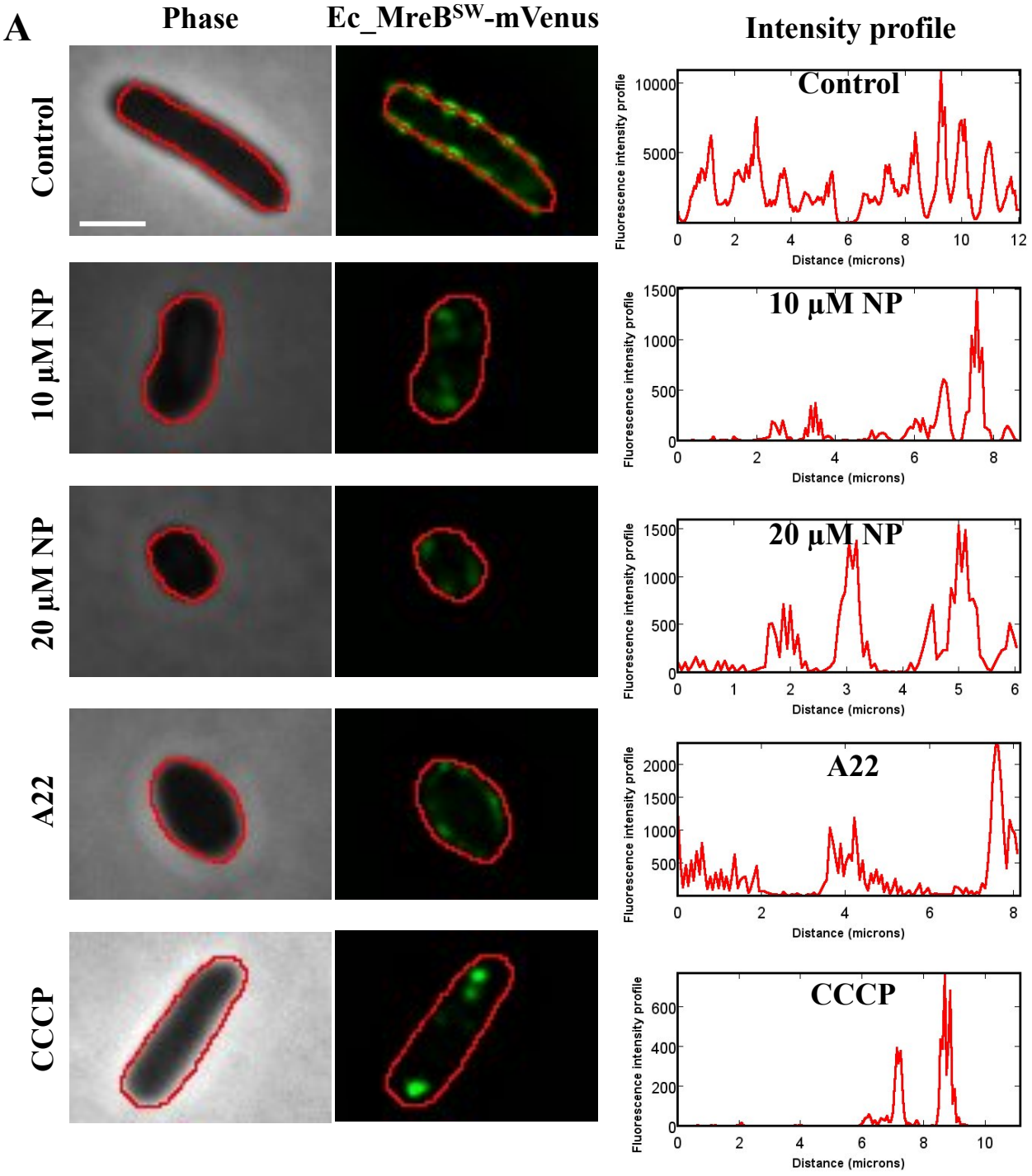

Fig. SI-9A.

Supplementary Figure 9

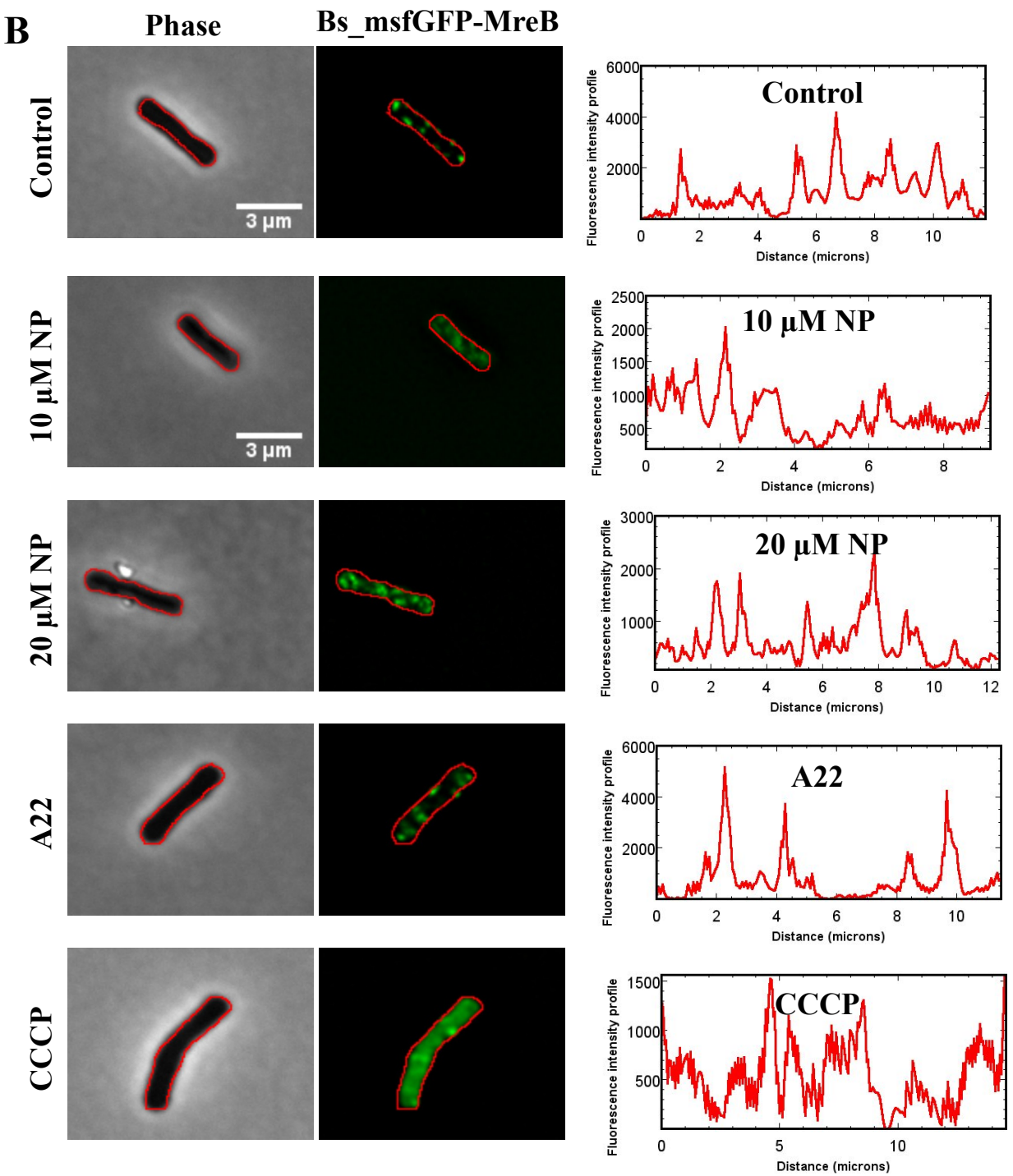

Fig. SI-9B.

Supplementary Figure 10

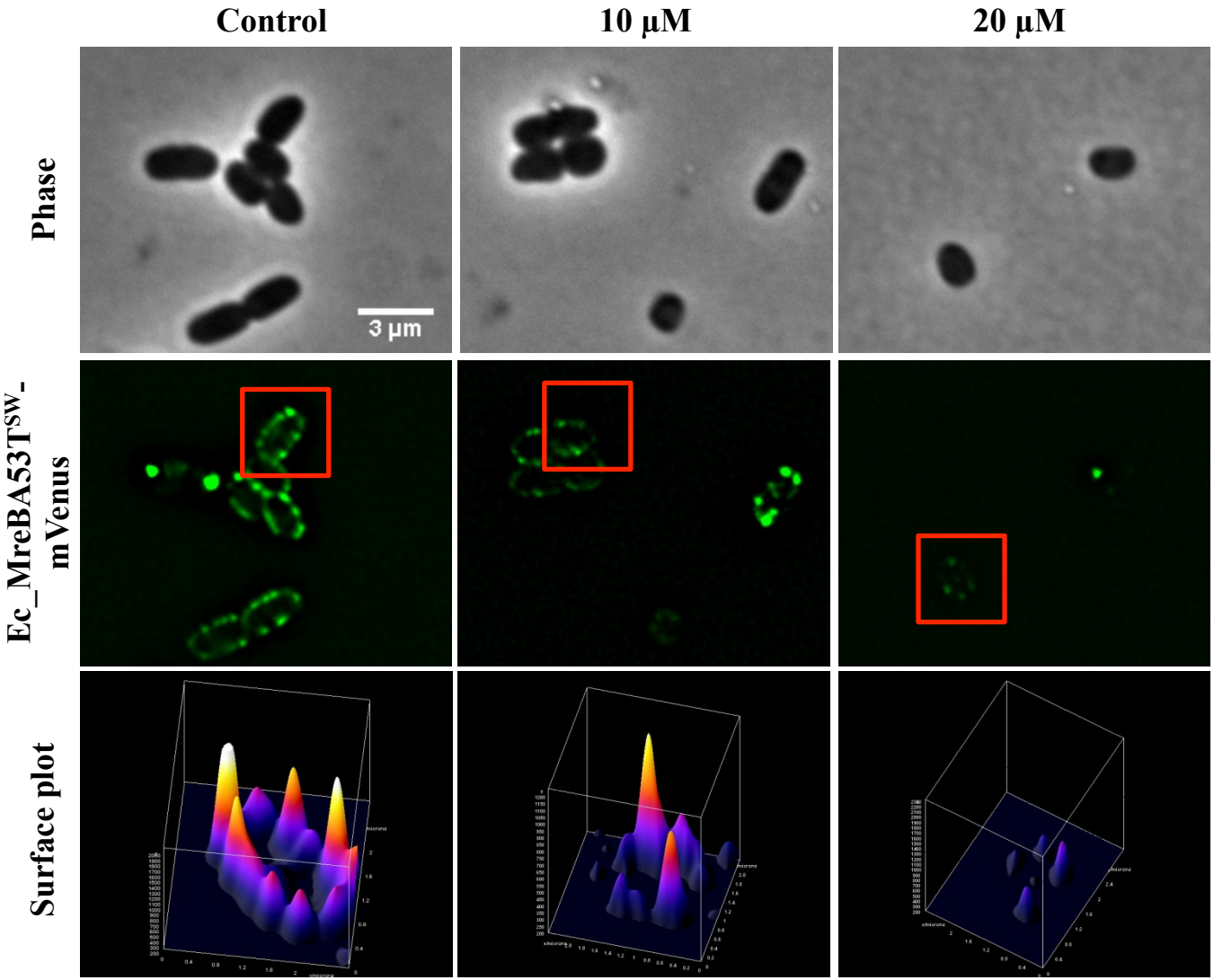

Fig. SI-10.

Supplementary Figure 11

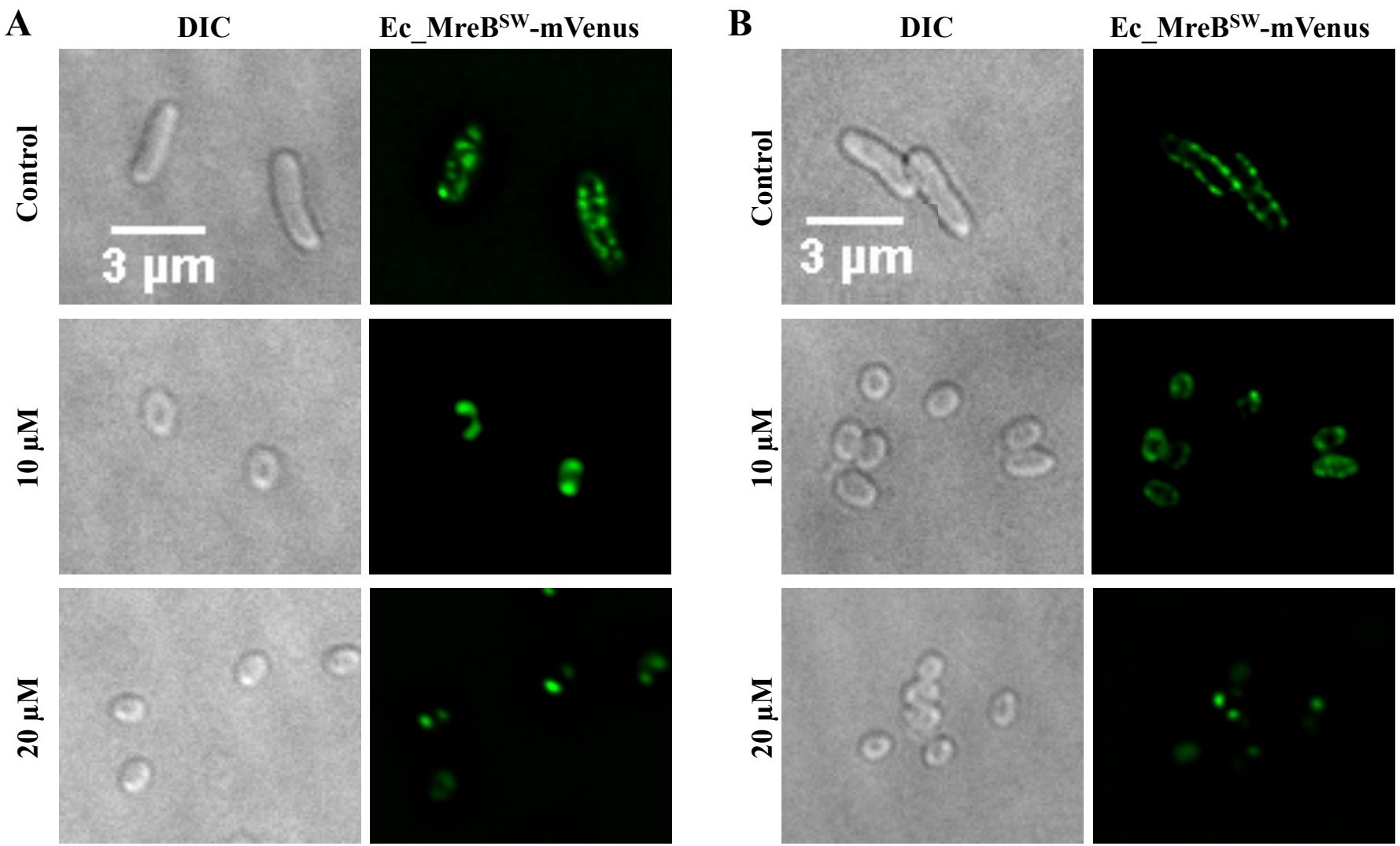

Fig. SI-11.

Supplementary Figure 12

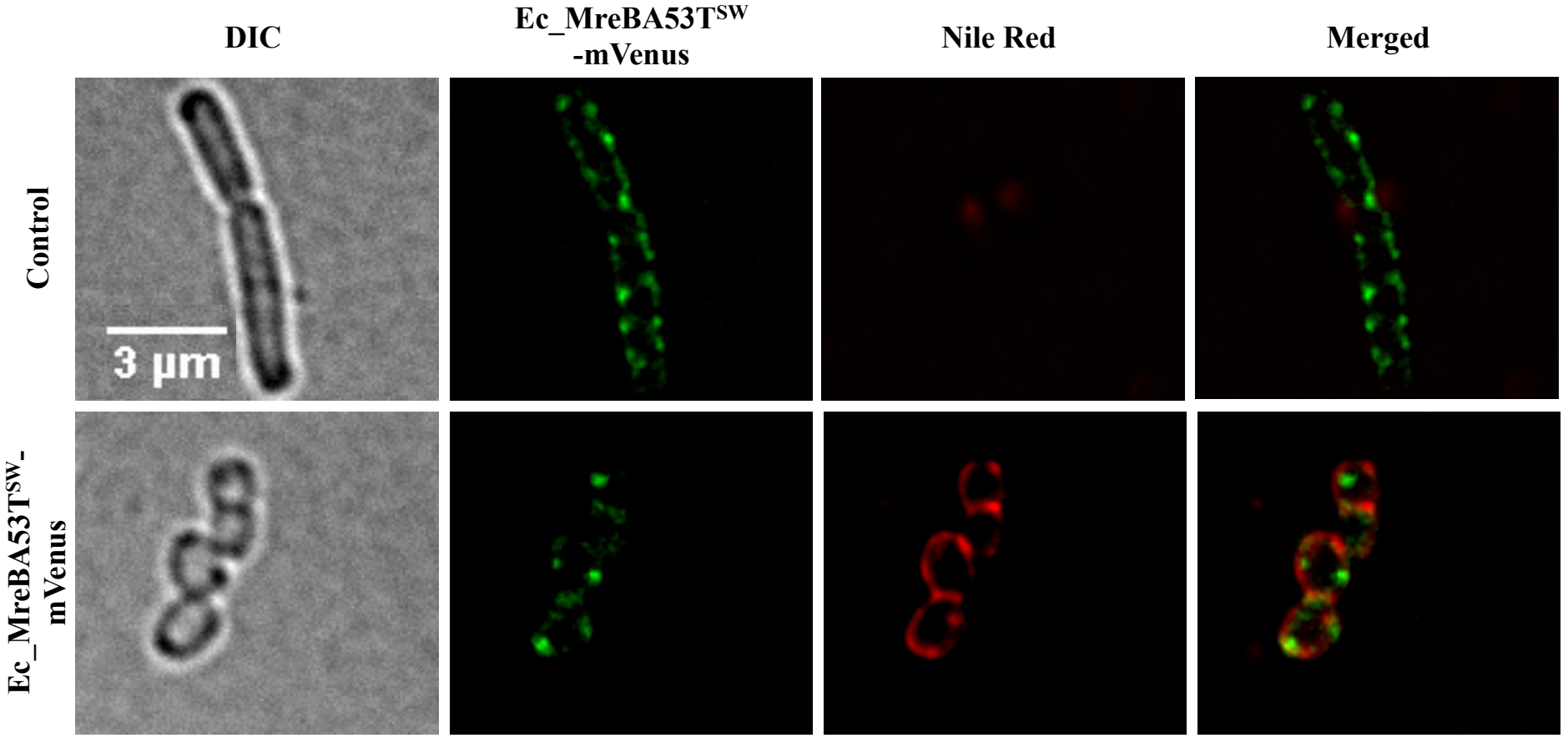

Fig. SI-12.

Supplementary Figure 13

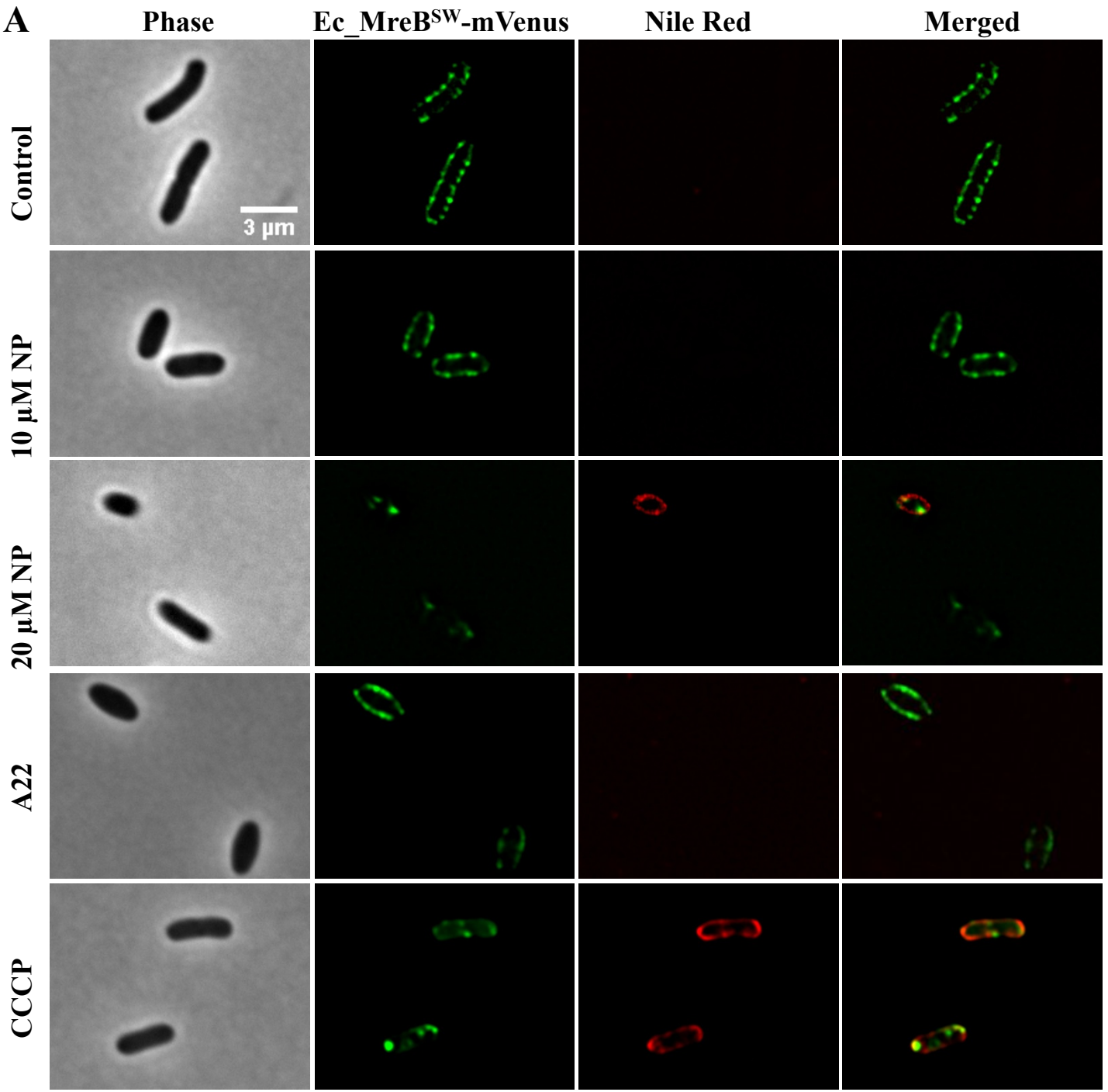

Fig. SI-13A.

Supplementary Figure 13

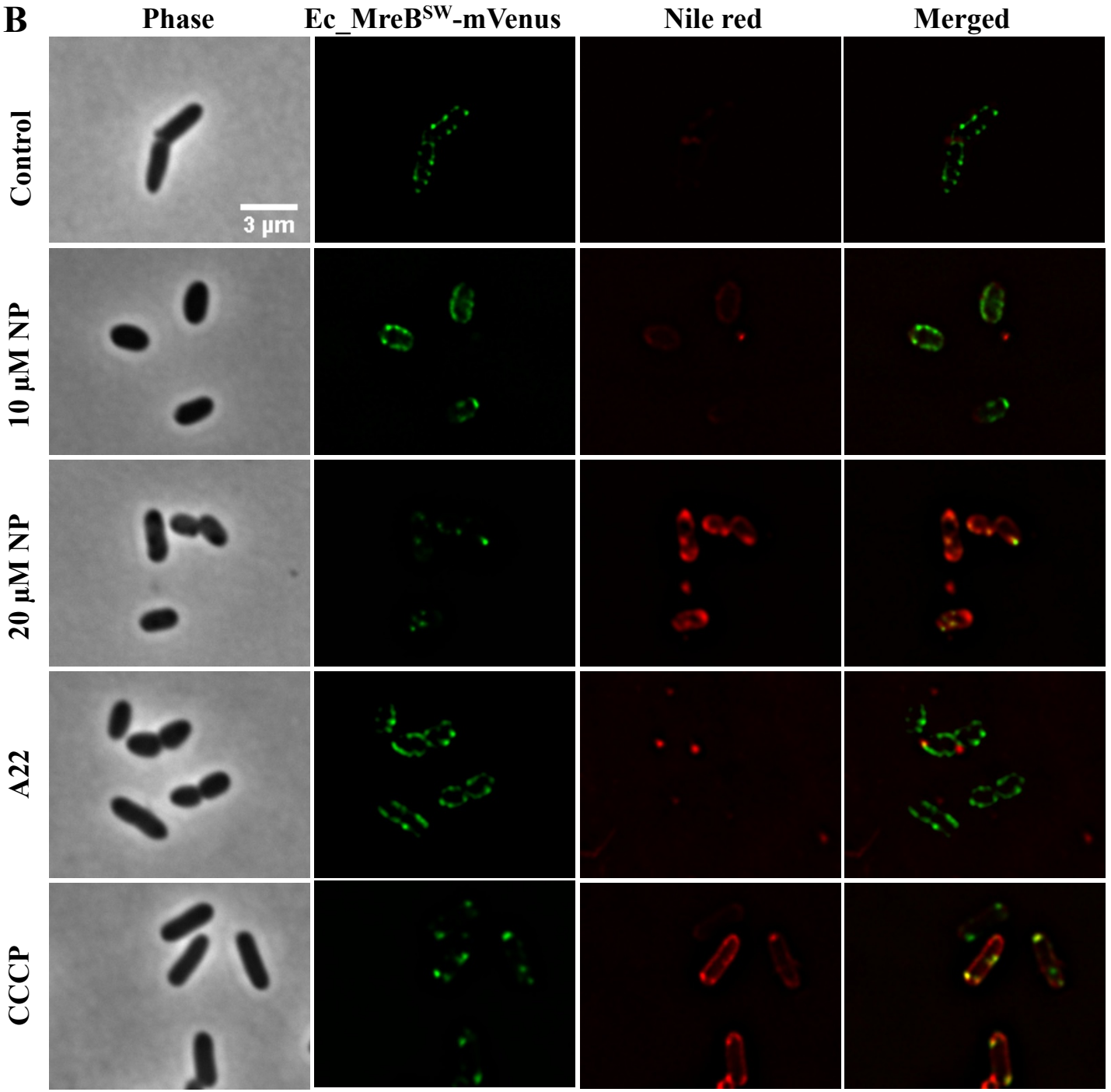

Fig. SI-13B.

Supplementary Figure 13

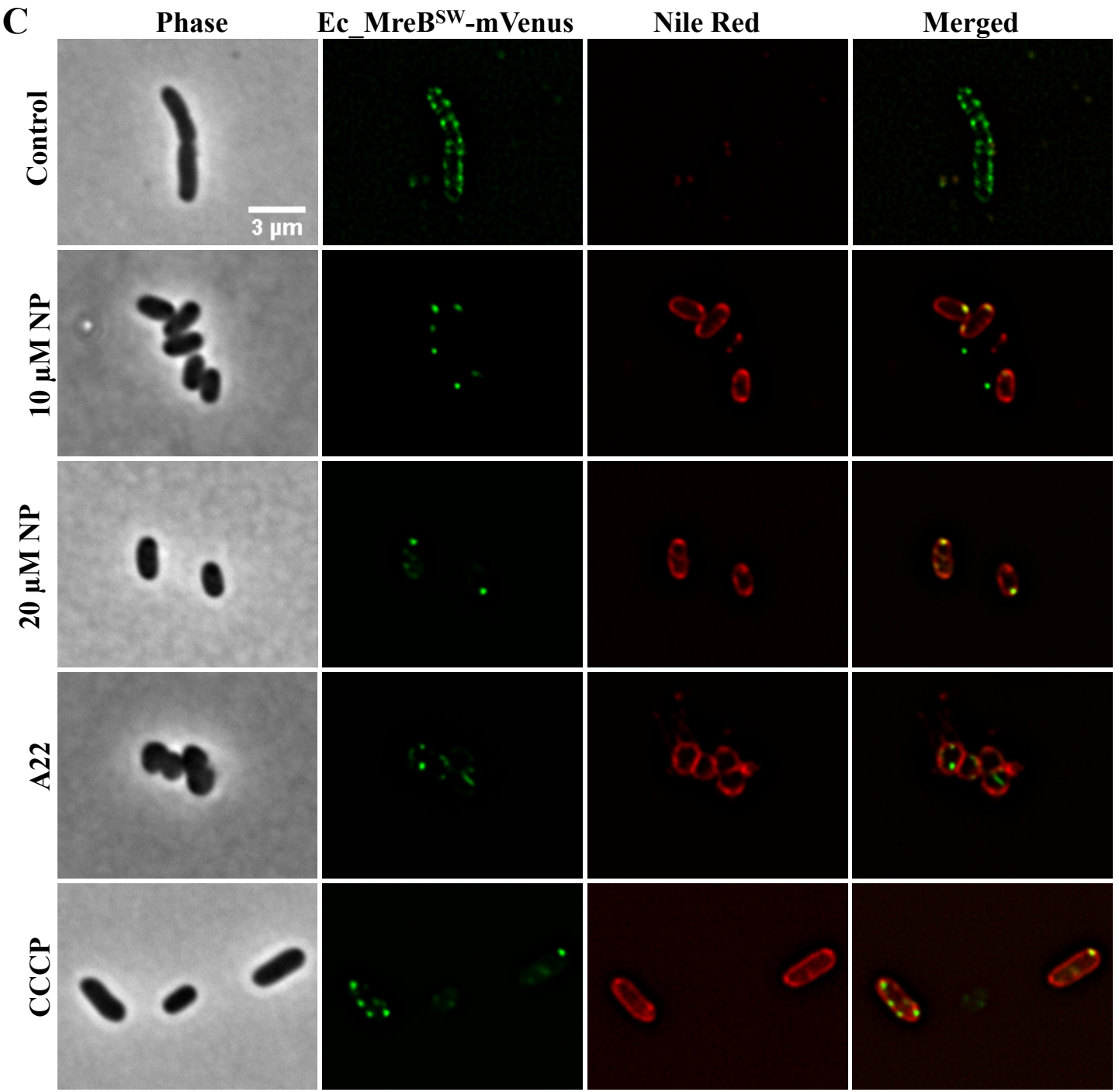

Fig. SI-13C.

Supplementary Figure 13

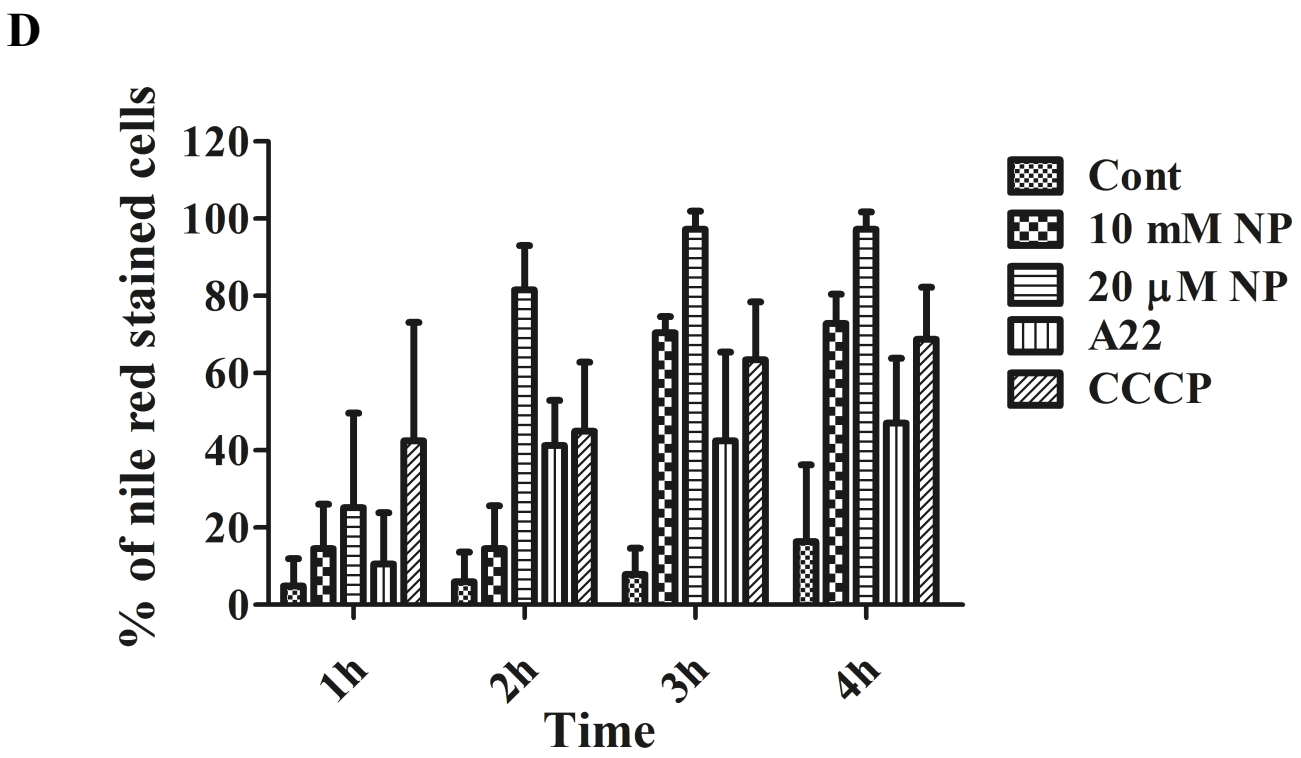

Fig. SI-13D.

Supplementary Table 1

Table SI-1

Plasmid/Strain	Description	Reference	Source
CCD1	*Escherichia coli* MG1655 Wild-type strain		Laboratory stock
CCD204	*Salmonella typhimurium* Wild-type strain		Laboratory stock
CCD3	*Bacillus subtilis* 168 Wild-type strain		Laboratory stock; Gift from R. Losick
CCD248	*Listeria monocytogens* Wild-type strain		Laboratory stock
CCD25	E. coli TZG - *wtftsZ::SD-ftsZ-gfp::Cm*	26	Akiko Nishimura
CCD291	REL606 MreB A53T (*E. coli*)	65	Kerwyn C. Huang
CCD292	REL606 MreB A53G (*E. coli*)	65	Kerwyn C. Huang
CCD374	*E. Coli* MG1655 *ΔdcrB::kan*	52	Manjula Reddy
CCD362	HS553 - *B. subtilis mreB:: msfGFP-mreB*	25	Henrik Strahl
CCD363	KS36 - *B. subtilis Ωneo3427 ΔmreB*	25	Henrik Strahl
CCD364	KS37 – *Δmbl::cat*	25	Henrik Strahl
CCD366	KS38 – *ΔmreBH::erm*	25	Henrik Strahl
CCD367	KS60 – *Ωneo3427 ΔmreB, Δmbl::cat, ΔmreBH::erm, Δrgl::spc*	25	Henrik Strahl
pCCD349	pRM-MreB^{SW}-mVenus - MreB^{SW}-mVenus under native mreB promoter cloned into pSC101	65	Kerwyn C. Huang
pCCD350	pRM-MreB^{SW}A53T-mVenus - MreB^{SW}A53T-mVenus under native mreB promoter cloned into pSC101	65	Kerwyn C. Huang
pCCD640	pDSW210-GFP-FtsA - GFP-FtsA under a weak IPTG inducible promoter, FtsA cloned into pDSW210	32	William Margolin
pCCD502	pTS37 - GFP-cJunLZ-EcMinD$_{MTS}$ under arabinose inducible promoter	33	Glenn King
pCCD434	pJSB2 - pBAD18 derivative with arabinose inducible promoter	27	Harold Erickson
pCCD436	pJSB100 – Ec_FtsZ under arabinose inducible promoter cloned into pBAD18 derivative	27	Harold Erickson